Journal of Fusion Energy, Vol. 2, No. 2, 1982

# Experimental Results from a Beam Direct Converter at 100 kV

W. L. Barr,[1] R. W. Moir,[1] and G. W. Hamilton[1]

Received December 3, 1981

A direct-energy converter was developed for use on neutral-beam injectors. The purpose of the converter is to raise the efficiency of the injector by recovering the portion of the ion beam not converted to neutrals. In addition to increasing the power efficiency, direct conversion reduces the requirements on power supplies and eases the beam dump problem. The converter was tested at Lawrence Berkeley Laboratory on a reduced-area version of a neutral-beam injector developed for use on the Tokamak Fusion Test Reactor at Princeton. The conversion efficiency of the total ion power was $65 \pm 7\%$ at the beginning of the pulse, decaying to just over 50% by the end of the 0.6-s pulse. Once the electrode surfaces were conditioned, the decay was due to the rise in pressure of only the beam gas and not to outgassing. The direct converter was tested with 1.7 A of hydrogen ions and with 1.5 A of helium ions through the aperture with similar efficiencies. At the midplane through the beam, the line power density was 0.7 MW/m, for comparison with our calculations of slab beams and the prediction of 2–4 MW/m in some reactor studies. Over 98 kV was developed at the ion collector when the beam energy was 100 keV. When electrons were suppressed magnetically, rather than electrostatically, the efficiency dropped to 40%. However, a better designed electron catcher could improve this efficiency. New electrode material released gas (mostly $H_2$ and CO) in amounts that exceeded the input of primary gas from the beam. The electrodes were all made of 0.51-mm-thick molybdenum cooled only by radiation. This allowed the heating by the beam to outgas the electrodes and for them to stay hot enough to avoid the reabsorption of gas between shots. By minor redesign of the electrodes, adding cryopanels near the electrodes, and grounding the ion source, these results extrapolate with high confidence to an efficiency of 70–80% at a power density of 2–4 MW/m. Higher power may be possible with magnetic electron suppression.

**KEY WORDS:** fusion; direct energy conversion; neutral beams.

## 1. INTRODUCTION

The intense neutral beams for every existing or presently planned fusion experiment will be produced from beams of positive ions. But, the conversion of positive ions into neutrals becomes less efficient as the energy is increased. At 100 keV for $D^+$ or 50 keV for $H^+$, the conversion efficiency is only 50%. At double those energies, it drops to 20%. Unless their energy is recovered in a direct converter, the unneutralized ions in the beam present a severe disposal problem as well as a waste of power. The obvious way to separate the ions out of the beam is by magnetic deflection after the beam leaves the neutralizer. The ion collector could be positively biased (if the electrons are suppressed) to recover part of the ion power electrically and to reduce the heat load on the collector. However, any system using a bending magnet would occupy a large volume for the magnet and ion dump (or collector), and would be incompat-

[1]Lawrence Livermore Laboratory, Livermore, California.



0164-0313/82/0400-0131$03.00/0 ©1982 Plenum Publishing Corporation

ible with the formation of a compact array of beamlines.

Several concepts for direct conversion have been or are being tested at various laboratories. The results of high-power beam direct conversion efforts at Livermore are analyzed in this paper and in more detail in ref. 1. High-power beam direct conversion and plasma (end-loss or diverter) direct conversion were reviewed in an earlier paper.[2] Recent plasma direct conversion results are described in ref. 3, while a design study of a beam direct converter for fusion reactors is given in ref. 4. The high-power beam direct converter design is a scaled-up version of a device[5] that we have successfully tested in Livermore at 15 kV in steady state. In those tests, either electrostatic or magnetic suppression of electrons worked equally well. The scale-up and the change from a steady state to pulsed operation introduced serious outgassing problems. These problems appear to be solvable by properly conditioning the electrodes. No further work on direct conversion is planned at Livermore due to a shortage of development funds.

At Fontenay-aux-Roses,[6] a circular 13-A, 70-keV neutral-beam injector was equipped with a "peripheral full beam energy recovery system." The ion source was held at ground potential and the neutralizer at negative high voltage. A long, gridded electron suppressor at the exit end prevented the escape of electrons from the negative neutralizer. Direct conversion of the unused ions was accomplished by collecting them near ground potential. The grid, about 0.7 m long, surrounded the beam immediately after the neutralizer. It was held 12–16 kV more negative than the neutralizer, and therefore also more negative than the space-charge neutralized beam (which was maintained within a few $kT_e/e$ of neutralizer potential by the electrons produced there). Ions in the outer part of the beam were extracted radially through the grid as they moved along it. The ion density therefore decreased with distance along the axis as the beam moved through the grid. As the density decreased, the grid potential was able to attract ions from deeper inside the beam. The grid was made long enough for the effect of the grid potential to finally be felt on the axis. Then, electron suppression was complete and electrons could not stream out of the neutralizer—even along the axis. The extracted ions passed out through the cylindrical suppressor grid and then through a planar, annular grid at the end before reaching the ion collector. To prevent excess heating of these grids, the pulse length was limited to about 0.2 s. Recovery efficiency of 45% of the energy of the full-energy ions was reported. This development effort has now been stopped.

At the Oak Ridge National Laboratory,[7] a perpendicular magnetic field is used to reduce the flow of electrons from the negative neutralizer to ground potential where the ions are collected. The novel feature here is that the entire region where the electric field is high (i.e., the region between the neutralizer and the ion collector) is immersed in the magnetic field. Preliminary results at up to 35 keV using the existing bending magnet set at a low value gave encouraging results. The difference in the drain on the accel power supply, when direct conversion is or is not used, indicating an efficiency of 80% for the energy recovery from the full-energy ions remaining after the neutralizer. If these results scale to higher voltages where the ion component becomes significant, this approach will be a very interesting one.

In independent efforts at Berkeley[8] and at Culham,[9] the concept of installing direct converters on individual beamlets was considered. The advantage of this concept was that electrons could be suppressed with relatively low voltage and ion collection with good optics, and therefore, with little loss. Ions could be collected outside the full beam.[8] The difficulty with this approach was that it required that the beamlets be well separated after leaving the neutralizer. This separation would reduce the average current density in the beam to uninterestingly low values unless the divergence of the beamlets was very small.

At Toshiba in Japan, the 200-keV, 32-MW, 110-s neutral-beam injectors[10] for the JXFR device are being designed with direct converters of the Livermore type. Numerical calculations of ion trajectories in the direct converter were done.

## 2. THEORY OF THE BEAM DIRECT CONVERTER (BDC)

Our BDC makes use of the fact that space charge, if not carefully neutralized, will cause the blowup and destruction of a positive ion beam. After the free electrons in the BDC are suppressed, the ions diverge away from the axis and strike collector electrodes outside of the normal path of the beam. Any fast-neutral component in the beam can pass through unaffected.

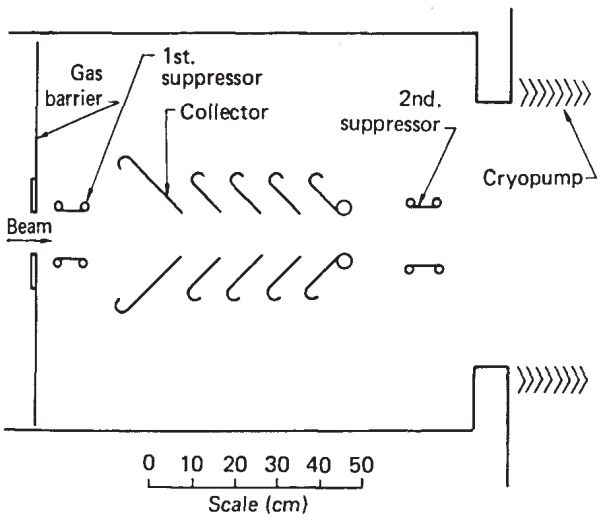


Fig. 1. The beam-direct converter electrodes, with electrostatic electron suppression.

Beam thickness, $d$, is an important parameter in determining the negative voltage required at the electron suppressor electrode. The applied voltage must produce a negative potential across the beam in spite of the positive space charge (of the beam where the electrons have been removed) and the positive potential due to the adjacent positive-ion collector. Because of the complex geometry (Fig. 1), we calculate the suppressor voltage numerically. However, the part of the potential due to space charge is approximately that of the ions in the beam, with the electrons removed. Poisson's equation in one dimension gives the potential difference $\Delta V$ between the center and the edges of a beam whose density profile is parabolic:

$$\Delta V = \frac{5(I/l)d}{32\varepsilon_0 v}$$

Here, $I/l$ is the ion current per unit of length normal to the beam axis, $d$ is the thickness of the beam, $v$ is the ion speed, and $\varepsilon_0$ is the permittivity of space. In the experiment, a negative 16 kV was required at the first suppressor, while the calculated space-charge effect was $\Delta V = 3$ kV, indicating that about $-13$ kV would be required at very low space charge.

## 2.1. Loss Currents

Any electron produced in the ion-collector region near the collector is attracted to it by its positive potential. Also, some of the secondary electrons produced by ion impact on the suppressors or on the walls of the vacuum tank reach the collector. This electron current not only reduces the efficiency by cancelling an equal amount of ion current, but also generates additional heat at the collector. Efficiency is also reduced by the power input to the suppressors to supply the current of the ions collected and the secondary electrons emitted by the suppressors. The loss current results from the production of cold ions and electrons as the beam passes through the background gas, from the direct interception of beam by the suppressors, and from the reflection of ions at the ion collector. The various loss processes are shown diagrammatically in Fig. 2. Both electrostatic and elastic reflection increase with increasing collector

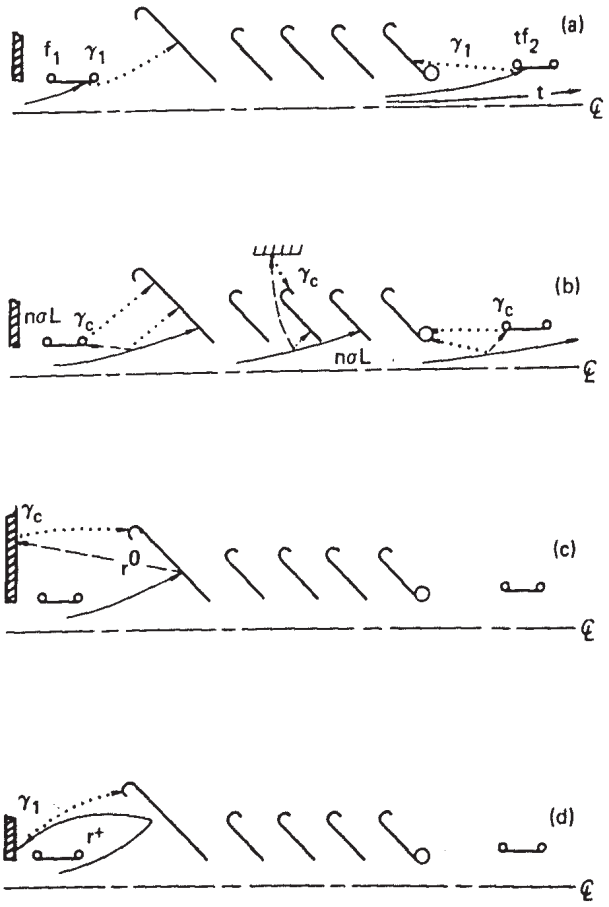


Fig. 2. The figure shows diagrammatically the generation of loss currents. Solid lines are beam ions. Dashed lines are cool ions. Dotted lines are electrons. Secondary electrons may be produced by beam ions bombarding the negative suppression electrodes (a) before or after the collector. Cold ions and electrons may be produced from the background gas (b) and attracted to the negative and positive electrodes where they produce secondary electrons. Beam ions may be reflected elastically (c) or electrostatically (d) from the positive collector, then producing secondary electrons.

potential. Electrostatic reflection results in the loss of ions and the collection of secondary electrons. Elastic reflection usually results in fast neutrals leaving the collector surface and secondary electrons returning. Also lost are those ions near the axis that pass through without being collected. This loss can be eliminated by operating the source and collector near ground potential and the neutralizer cell at negative high voltage. Ionization by either a fast ion or a fast neutral produces an ion-electron pair. Computer trajectory calculations show that all electrons strike the positive-ion collector, but only some of the cold ions strike a suppressor. Charge exchange by a fast ion results in a fast neutral and therefore the loss of an ion that would have been collected. It also produces a cold ion that we assume falls onto a suppressor and releases $\gamma_c$ secondary electrons that go to the ion collector. Stripping of a fast neutral produces a fast ion and an electron, both of which go to the ion collector and produce no net current.

By combining these loss currents, we obtain an expression for the net collected current $I_c$ and the drain currents $I_1$ and $I_2$ at the two suppressors per unit of beam current $I^+$ of any one ion species:

$$I_c/I^+ = 1-\left[ f_1(1+\gamma_1)+n\sigma L(1+\gamma_c)+r^0\gamma_c + r^+(1+\gamma_1)+t(1+f_2\gamma_1)\right]$$

$$I_1/I^+ = f_1(1+\gamma_1)+n\sigma L(1+\gamma_c)f_{1c} +\left[ r^0\gamma_c + r^+(1+\gamma_1)\right] f_r$$

$$I_2/I^+ = n\sigma L(1+\gamma_c)f_{2c} + tf_2(1+\gamma_1)$$

Here, $f_1$ and $tf_2$ are the fractions of the incident beam that are intercepted by suppressors 1 and 2, respectively. $f_{1c}$ and $f_{2c}$ are the corresponding quantities for the cold ions, $f_r$ is the fraction for reflected ions striking the first suppressor, while $t$ is the fraction of the beam that passes completely through the collector. $t$ varies with the ratio of the collector voltage to beam energy. These five fractions can be determined either from our trajectory calculations or from the experimental data. The quantity $n\sigma L$ represents the product of the neutral gas density and the sum of the integrals of the ionization and charge exchange cross-sections over the path lengths. The neutral component of the beam, multiplied by the neutral-to-charged ratio, is included in the ion term. The cross-sections vary with ion energy and ion energy varies with position, because of the potentials. This sum of integrals, then, varies with collector voltage and beam energy. The reflection coefficients $r^0$ (elastic)[11] and $r^+$ (electrostatic) both increase rapidly as the collector voltage approaches beam energy. If fractional energy ions are present in the beam, their effect is mainly to increase the reflection coefficients for collector potential near or above their energies. Finally, $\gamma_1$ and $\gamma_c$ are the secondary electron emission coefficients for beam ions and for the cooler reaction products, respectively. $\gamma_1$ and $\gamma_c$ vary with impact energy and with surface conditions.

In principle, both $f_1$ and $f_2$ can be made to vanish, and the loss due to $t$ can be eliminated (by using a grounded source and a negative neutralizer). The $n\sigma L$ term and the $\gamma$'s can be solved for, since $r^+$ and $r^0$ are only important when the collector potential is nearly equal to the beam energy. The above equations therefore establish an upper limit on the gas density that can be tolerated. Since typically, $n\sigma L \sim 800p$ in our tests with $p$ in Torr, and $\gamma_c \sim 3$, the requirement is that $p \ll 3\times 10^{-4}$ Torr. Experimentally, we observe large loss currents comparable to the total ion current whenever $p \sim 1\times 10^{-4}$ Torr.

Secondary electron emission at the ion collector can be important. At high beam current, the potential immediately in front of the collector can be greater than $V_c$. In that case, electrons emitted from the collector accumulate and modify the potential to produce a Boltzmann distribution with potential relative to $V_c$:

$$n_e = n_{e0}e^{e(V-V_c)/kT_e}$$

where $n_{e0}$ is equal to the maximum ion density at the collector surface, and $T_e$ is the electron temperature. This electron density prevents the potential from rising more than a few times $kT_e/e$ above $V_c$. As a result, the potential rises more rapidly, but to a plateau at $V \sim V_c$, increasing the electric field near the suppressor. Therefore, the negative potential, $-V_{sup}$, required at the suppressor scales with space charge as

$$V_{sup} \propto (M/W)^{1/2}(I/l)d$$

The practical upper limit to the beam current is determined by the first suppressor electrode. As the current is increased, the electric field becomes stronger, requiring higher $V_{sup}$ and causing a more rapid divergence of the ions. To prevent the suppressor from intercepting fast ions, it must be moved

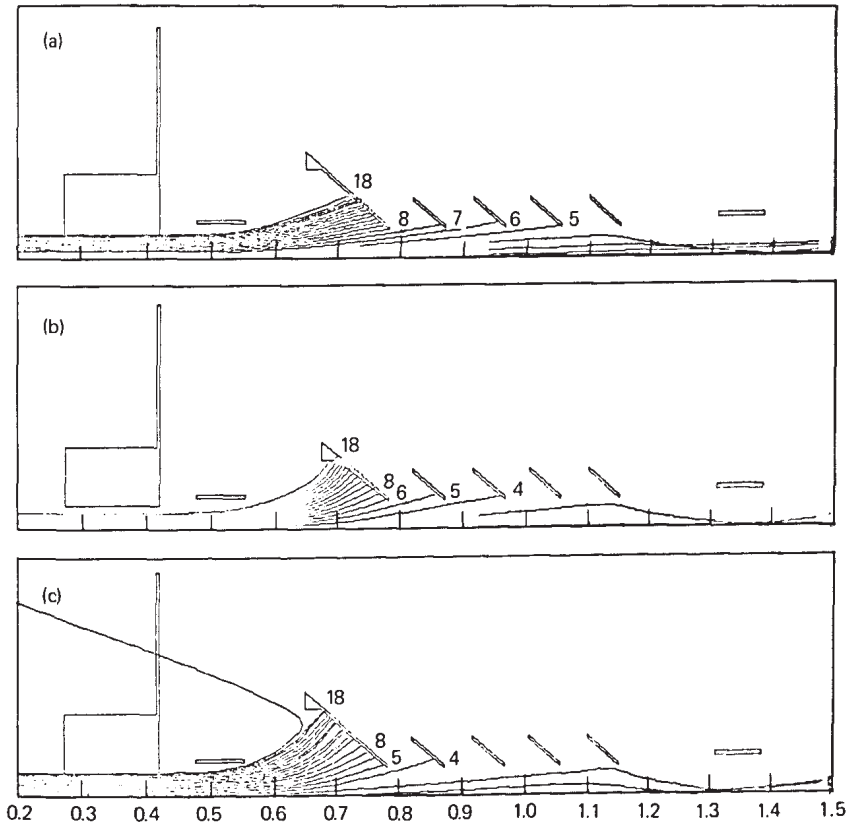


**Fig. 3.** Trajectories of 100 keV $He^+$ ions calculated at three different current densities: (a) 5 A/m, (b) 10 A/m, and (c) 14 A/m; in the geometry tested with electrostatic suppression. The potentials are: $V_1 = -20$ kV, $V_c = +95$ kV, $V_2 = -10$ kV.

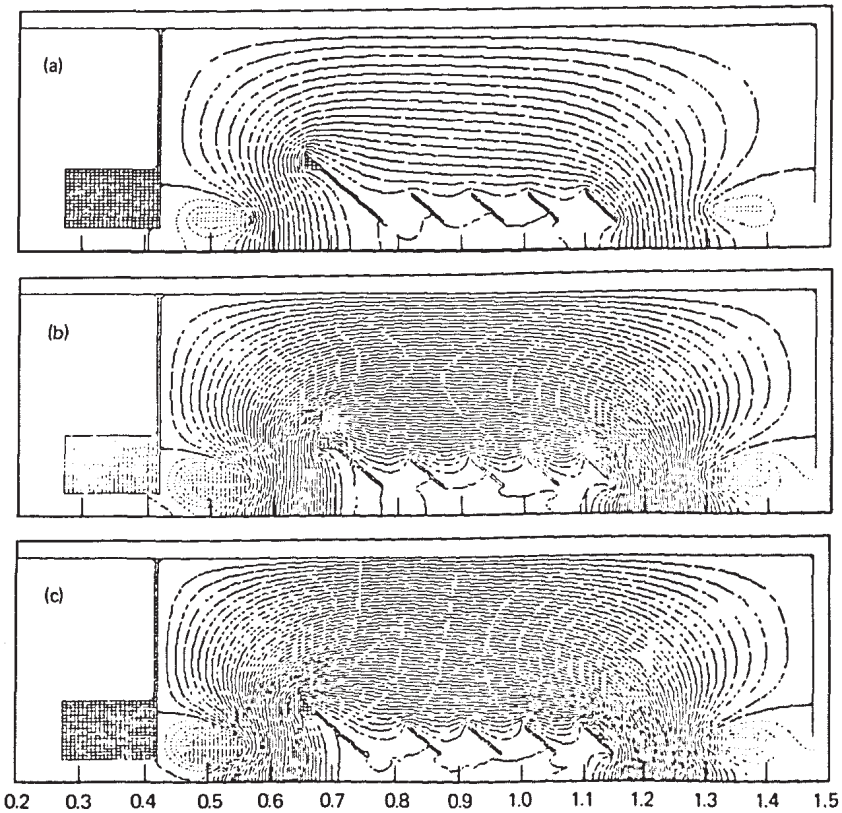


**Fig. 4.** The calculated equipotential contours for the three cases shown in Fig. 3. Notice the advancement of the meniscus in the throat of the collector as the current is increased.

further from the beam and (or) shortened, again requiring higher $V_{sup}$. The practical current density limit is finally set by the power loss and the resulting heat at the suppressor.

The effect of increasing the current density of the ions in the beam is shown in Figs. 3 and 4, which were generated by computer simulation. Figure 3 shows ion trajectories and Fig. 4 shows the equipotential surfaces calculated for three different current densities but the same geometry as used in the tests. Higher suppressor voltage is required for higher current, as discussed above, but for comparison purposes, the voltages were held fixed in Figs. 3 and 4. The code calculates the trajectories of beam ions and cold ions in the self-consistent potential produced by the applied voltages plus the space charge of both species of ions and electrons.

## 3. THEORY OF MAGNETIC SUPPRESSION OF ELECTRONS

Some of the problems with electron suppression are reduced if a magnetic field is used instead of a potential barrier to stop the electrons as suggested by O. B. Morgan of ORNL.[7] In particular, it should be possible to handle beams of greater thickness with magnetic suppression. The difficulty with the use of a magnetic field comes from having to avoid regions where discharges can occur in the electric and magnetic fields.

In our tests, we use a localized perpendicular magnetic field and attempt to minimize the strength of the fringing field at the location of the ion collector. The electric field produced by the collector potential sweeps out all electrons from regions where electron trajectories intercept the collector. This electron-free region is the sheath across which most of the difference in potential is developed and its location is determined by the scale of the electron trajectories. As discussed earlier, space-charge effects near the collector determine the magnitude of the electric field there. This set of conditions determines the location and thickness of the sheath from which the ions diverge out of the beam and strike the collector.

It is also necessary that the sheath be stable enough to prevent any appreciable electron current from flowing to the ion collector. A catcher must exist at a low positive potential to catch electrons that become trapped by the magnetic field and prevent them from reaching the high positive potential of the ion collector. In order to collect the electrons at low potential, the catcher electrode is designed to fit closely around the beam just after it passes through the magnet (Fig. 5). By partially shielding out the strong electric field, it provides a region where electrons can be removed from the beam by $E \times B$ motion. Electron orbit size in the drift region is given by

$$r_e = mE/eB^2$$

and these orbits must remain much smaller than the dimensions of the catcher. Therefore,

$$E/B^2 \ll 2\times 10^{10}\ \text{V/m}-\text{T}^2$$

In the sheath, $E = 10^6$ V/m, requiring a magnetic field strength much greater than $2\times 10^{-3}$ T (20 G). Also, for one end of the catcher to collect the electrons at a low positive potential, that potential must be at least as positive as the region in the beam from which the electrons are removed. To the extent that the strong electric field is shielded out, the potential in the beam is nearly the same as the inner walls of the catcher to which they are linked by magnetic field lines. For that reason, part of the inner side walls of the catcher are held at a lower potential than the outer walls and ends. Figure 5 shows the assembly.

Electrons can enter the sheath and be accelerated into the ion collector if the electric field inside the catcher electrode is either too strong or is in the wrong direction. The polarization electric field $E_p$ that results from the separation of electrons and ions is in the direction to produce an $E_p \times B$ drift toward the collector. If $E_p$ becomes too strong, many of the electrons will go to the ion collector rather than to the end of the catcher. $E_p$ can be estimated from the density, $n_e$, of electrons and the displacement distance $d$:

$$E_p \approx \frac{n_e e d}{\pi \varepsilon_0}$$

This gives $E_p \approx 1\times 10^5$ V/m when $n_e$ is $1.4\times 10^{14}$ $\text{m}^{-3}$ (the mean beam ion density in our tests) and $d = 0.1$ m is the thickness of the beam. The electric field inside the catcher must be $\sim 10^5$ V/m in order to remove the electrons. Therefore, $E_p$ is significant and can even become dominant if $n_e$ should increase. Any increase in the density of gas in the region or the secondary electron emission coefficient would increase $n_e$ since it is determined by the balance between production and loss rates.

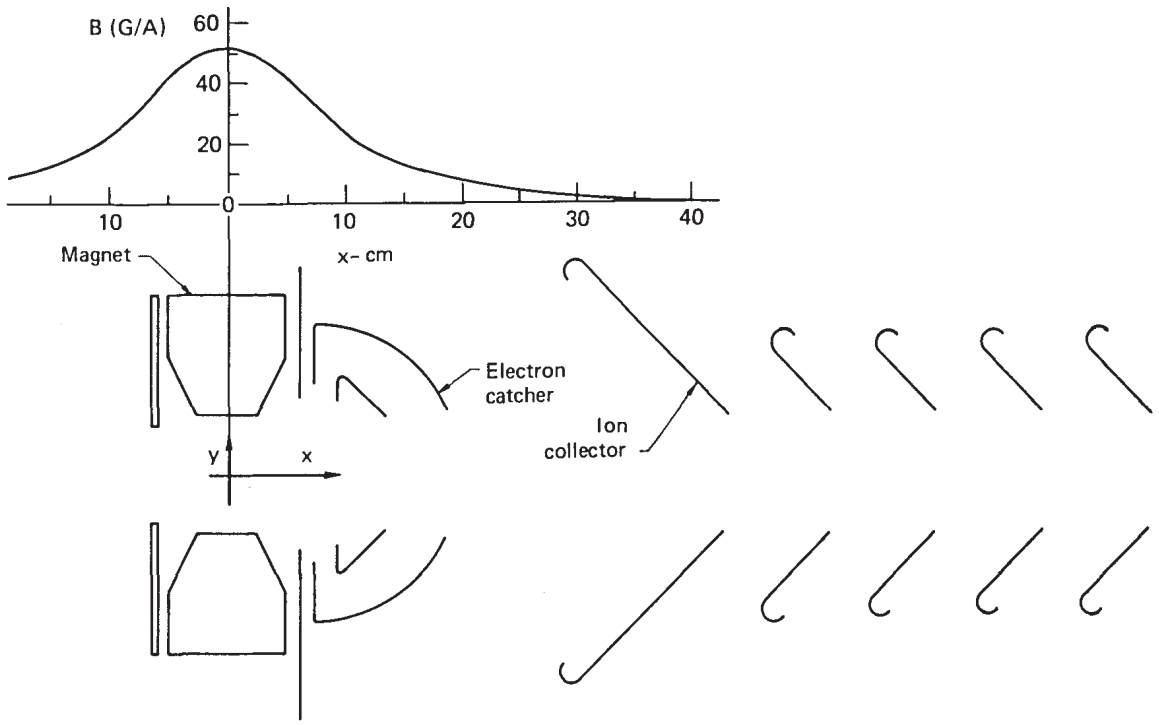


Fig. 5. Magnetic field strength in the direct converter using magnetic electron suppression. Best results were obtained with a peak field of 100 to 150 G.

Electrons might also be able to escape from the catcher and enter the sheath if a turbulent electromagnetic field can couple enough energy into the electrons. The situation here is similar to that in the sheath in theta pinch experiments for which the stability analysis exists.[12] The difference here is due to the finite width of the beam and the consequent polarization that results from the displacement of the electrons. Using the theta pinch analysis as a guide, it appears that any one of the three modes, ion acoustic, modified two-stream, or Buneman, could increase the electron temperature and allow electrons to enter the sheath.

## 4. EXPERIMENTAL ARRANGEMENT

Figure 6 shows a schematic of the beamline as it was modified for testing the BDC. The BDC was located beyond the huge spherical pumping reservoir from the source so that it could be isolated by a valve. To maximize the full-energy ion component of the beam, the neutralizer section of the beamline was reduced to the minimum length possible. However, the short neutralizer resulted in the incomplete neutralization of space charge in the beam, and the increased beam divergence caused a smaller fraction of the beam to pass through the aperture into the BDC.

The decision to shorten the neutralizer was made after calculations showed that the line density, $\pi$, of gas molecules between source and BDC could be reduced from $\pi = 7\times10^{15}$ to $1\times10^{15}$ cm$^{-2}$. For 100-keV $He^+$, where $\sigma_{10} = 2.2\times10^{-16}$ and $\sigma_{01} = 0.9\times10^{-16}$ cm$^2$, reducing $\pi$ should double the ion fraction of the beam from 0.4 to 0.8. For 100-keV $H^+$, there was little to be gained because most full-energy ions would survive in either case. But, 0.7 of the 100-keV $H_2^+$ should reach the BDC if $\pi$ is reduced, while only 0.1 should reach it if $\pi$ had the larger value. Of greater concern was the effect of the large half-energy ion current that would result from the dissociation of $H_2^+$ with the larger value. Another modification to the beamline was the installation of a retractable aperture in the sphere to remove any halo from the beam and reduce the generation of gas at the entrance to the BDC.

A cryopump[13] was mounted directly after the BDC to reduce the gas flow back from the beam dump. The pump contained argon jets to provide the sorptive medium for pumping helium. Pumping speeds were $8\times10^4$ liters/s for $H_2$ without argon, and $5\times10^4$ liters/s for He with a flow of about 20 argon atoms per helium atom pumped. The base

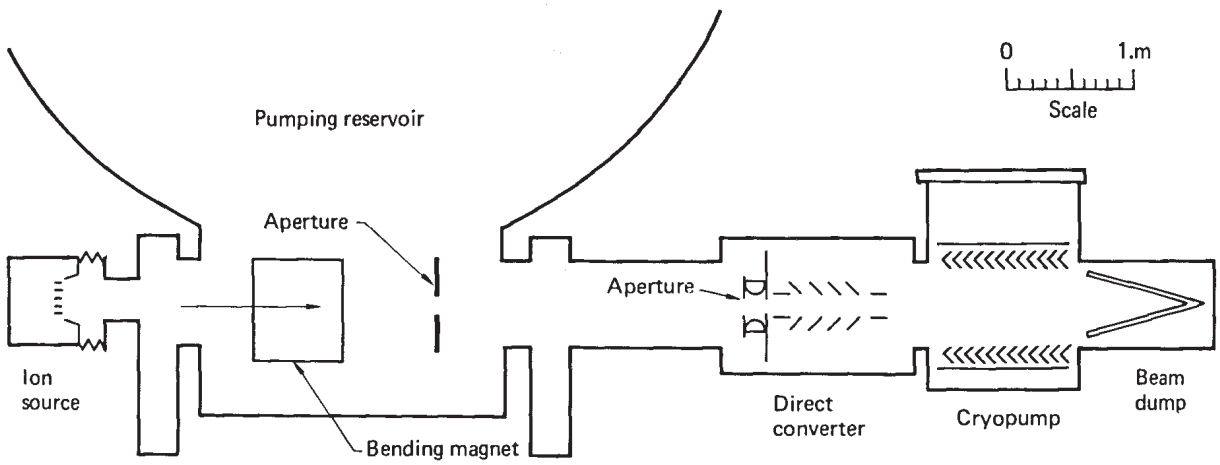


Fig. 6. The direct converter mounted on the beamline with the neutralizer gas cell removed.

pressure in the BDC was $4\times10^{-8}$ Torr; about one order of magnitude lower than is normal on the beamline.

The dimensions of the BDC are dictated by the size and density of the beam. At the location of the front aperture on the BDC, 5.4 m from the source, the beam has near-Gaussian profiles both vertically and horizontally. The $1/e$ half-widths were expected to be 4.7 cm horizontally and 14 cm vertically. Near the end of the neutralizer cell where the BDC would be located on an operating neutral-beam injector (i.e., about 2 m from the source), the beam profile is flat topped. There, a full sized LBL source produces a profile that can be more nearly approximated by the two-dimensional slab geometry assumed in our computer calculations. Partly to increase the aspect ratio of the beam profile inside the BDC at the 5.4-m location, we chose a rectangular aperture 8.85 cm wide and 35.5 cm high. We calculated that 81% of the beam should be able to pass through the aperture and enter the BDC. The measured fraction of the beam that was transmitted by the aperture turned out to be only 0.26 for H and 0.36 for He because of the greater beam divergence that resulted from the removal of the neutralizer cell, as discussed above.

## 5. EXPERIMENTAL RESULTS USING ELECTROSTATIC SUPPRESSION

The first data were taken using a helium beam so that the evolved gases could be distinguished from the primary gas from the beam. The electrical circuit that was used for electrostatic suppression is shown in Fig. 7. The collector voltage, $V_c$, was generated by the flow of the net collector current, $I_c$, through the variable load resistor, $R$, and was therefore directly proportional to $I_c$. The values of the suppressor voltages $V_1$ and $V_2$ that were required to suppress the electrons were determined by observing $I_c$ as these voltages were varied. Figure 8(a) shows the measured currents $I_c$, $I_1$, and $I_2$ plotted against $V_1$ with $V_2$=

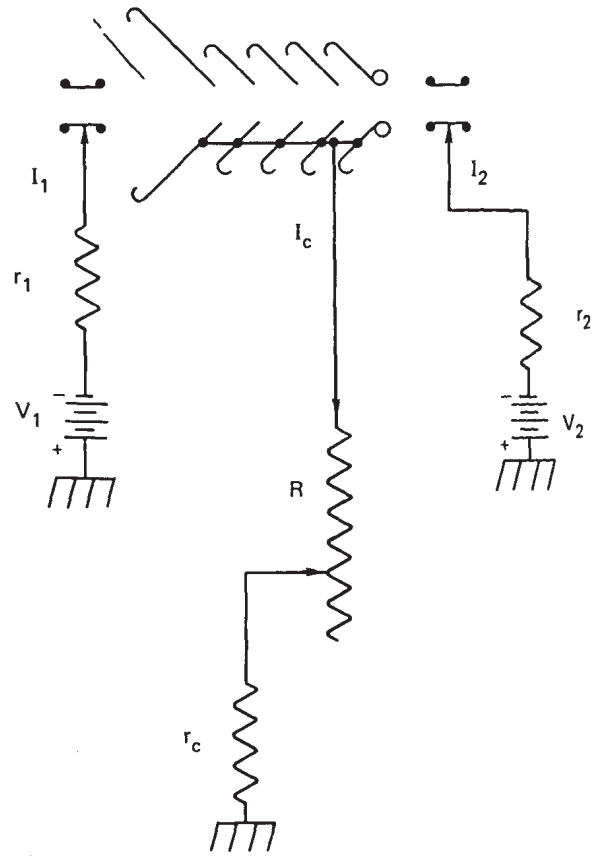


Fig. 7. The electrical circuit used with electrostatic electron suppression.

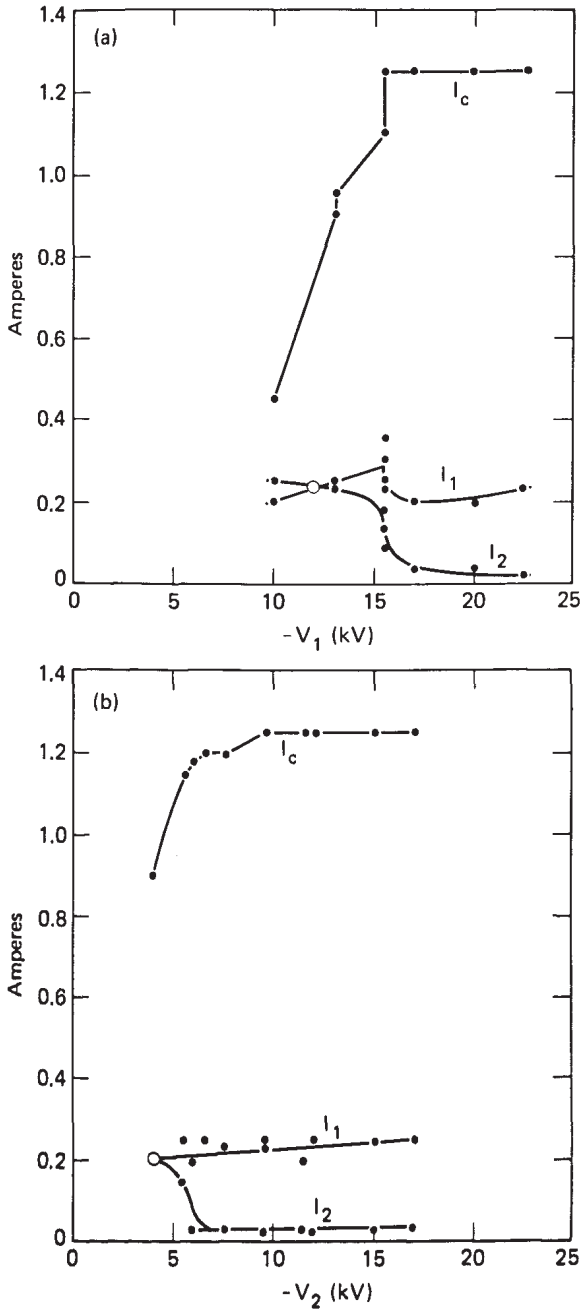


Fig. 8. This figure shows the variation of the collector current ($I_c$) and the suppressor currents ($I_1$ and $I_2$) as the suppressor voltages are varied. In (a), $V_2 = -11.5$ kV. In (b), $V_1 = -20$ kV. $V_c$ varied up to +86 kV in both. It is apparent that $-V_1 > 16$ kV and $-V_2 > 6$ kV are required. The indicated suppressor currents were measured late in the pulse when the pressure was high.

$-11.5$ kV, and Fig. 8(b) shows the currents plotted against $V_2$ with $V_1 = -20$ kV. It can be seen in the figure that $-16$ kV is required at the first suppressor and $-6$ kV at the second when the collector voltage $V_c = 86$ kV. To allow for $V_c \simeq 100$ kV, we typically applied $-20$ kV and $-11$ kV at the two suppressors. It can be seen that $I_2$ decreases sharply as $-V_1$ is increased through the required value of 16 kV. This is because the transmitted ion beam decreases sharply when $V_1$ is effective. $I_2$ also decreases sharply when $-V_2$ is raised through its required value of 6 kV, because when $V_2$ is ineffective, $V_c$ drops and the transmitted beam increases due to the reduced space charge blowup of the beam. These data were taken with $R = 69$ kΩ so that $V_c$ varied up to 86 kV and $I_c$ varied up to 1.25 A. (Beam dump calorimetry measured 1.42-A $He^+$ and 0.35-A $He^0$ through the BDC during the first part of the tests. This changed to 1.02-A $He^+$ and 0.76 A $He^0$ for the remainder of the tests.)

The improvement in the performance of the BDC as the electrodes cleaned up was remarkable. Figure 9 compares the observed variation of $V_c$ during a pulse on the first day of consistent operation with the variation during a pulse two weeks later. The rise in total pressure improved by only about a factor of one-half (to about $2 \times 10^{-5}$ Torr) during that period, but the amount of evolved $H_2$ and CO improved by at least an order of magnitude. Therefore, the composition of the gas and the calibration factor for the ion gauge varies during a pulse, distorting the indicated pressure variation. The residual gas analyzer (RGA) indicates that with a He beam the pressure of He rises nearly linearly with time, while those of $H_2$ and CO rise faster early in a pulse but then flatten off as they approach their equilibrium values. After the pulse, $H_2$ is pumped out the fastest and He the slowest by the cryopump. Possibly more important than the reduction of gas pressure is the reduction of the secondary electron emission from the various surfaces.

It is important to note that the sag in $V_c$ and $I_c$ during a pulse was limited. That is, the sag disappeared when $R$ was increased until the smallest value of $I_c$ at any time during the pulse was sufficient to develop a voltage $V_c$ nearly equal to the accel voltage. Also, in that case, the $V_c$ and $I_c$ signals were very

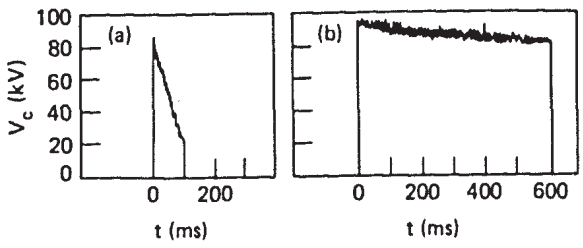


Fig. 9. This figure compares the variation with time during a pulse in the voltage developed on the collector: (a) before and (b) after conditioning the electrodes.

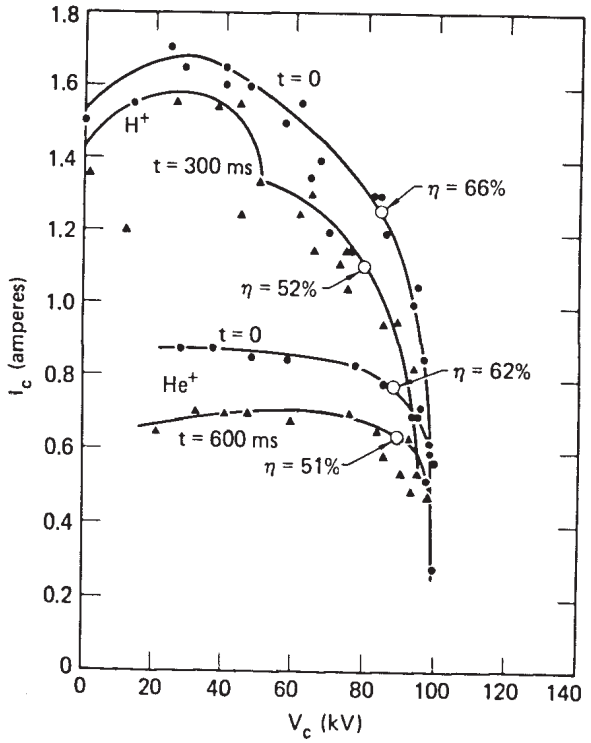


**Fig. 10.** Measured collector current $I_c$ vs collector voltage $V_c$ for a helium beam and for a hydrogen beam, both using electrostatic suppression. Dots indicate data taken at the beginning, and triangles data taken at the end of the pulse. The points of maximum efficiency are indicated. Half energy ions are evident on the hydrogen curve.

clean, indicating that the noise was not due to variations in accel voltage or to sparking in the BDC.

Figure 10 shows the measured characteristic curve, $I_c$ versus $V_c$, for the BDC with electrostatic suppression at the beginning and at the end of a 600-ms pulse with a helium beam. The indicated efficiency, $\eta$, of the BDC was obtained by choosing the maximum product $I_c \times V_c$, from the curve, subtracting the power supplied to each suppressor, and dividing by the total ion power into the BDC. We determine the total average ion power calimoretrically by noting the difference in the heating of the beam dump when a bending magnet is turned on. With a $He^+$ beam, the efficiency was 62% at the beginning and 51% at the end of the pulse in this run. Partly, the decrease during a pulse was due to increased production of cold ions and electrons that decreased $I_c$ and $V_c$ and increased the power consumed by the suppressors. Also, the decrease was due partly to the loss of ions due to the increased rate of charge exchange as the gas density built up. The calorimeter measured only the average beam power during a pulse.

Figure 10 also shows the measured $I_c$ versus $V_c$ curve for a hydrogen beam, again using electrostatic suppression of electrons. These data were taken on the first day of operation with a hydrogen beam after the electrodes were conditioned with a helium beam. No new conditioning of the electrodes was required, and in fact, performance appeared to degrade slightly with further operation with the hydrogen beam, apparently as hydrogen was reabsorbed in the cooler parts of the electrodes.

With hydrogen, the maximum current measured at the BDC was 1.7 A of ions and the total ion power measured calorimetrically was 158 kW. No measurement was made on the composition of the beam while the BDC was on the beamline, but by assuming that the extracted beam was 47% $H^+$, 37% $H_2^+$, and 16% $H_3^+$, we calculated the composition of the beam through the BDC to be 1.4 A of 100-keV $H^+$, 0.04 A of 67-keV $H_2^+$, 0.24 A of 50-keV $H^+$, and 0.11 A of 33-keV $H^+$. This would account for the 158 kW of ion power but would give 1.8 A of total ion current instead of the observed 1.7 A. The noise on the BDC data prevented the direct measurement of the beam composition, but it suggested a composition similar to the predicted one (see Fig. 10). The efficiency of direct recovery using electrostatic electron suppression and the hydrogen beam was 66% of the total ion beam initially, but dropped to 52% by the end of a 300-ms pulse. If only the full energy ions are considered, the efficiency was 74% early and 59% late in the pulse. Actually, part of the 12 kW of drain on the suppressor supplies was due to the reflected fractional energy ions, so that without them, the efficiency should be higher than 74%. The uncertainty here is probably about $\pm 7\%$ as was observed with the $He^+$ beam where one $I_c$ versus $V_c$ scan yielded $\eta = 77\%$.

## 6. RESULTS USING MAGNETIC SUPPRESSION

In order to test our concept of magnetic suppression, the first suppressor was replaced with an electron catcher shown in Fig. 5. The curved sides were made of 0.51-mm-thick molybdenum with no cooling other than by radiation. The end plates and the support were made of 304 SS. The figure also shows the magnetic field strength as it varied with distance through the electron catcher and ion collector. Figure 11 shows the electrical circuit that used a stack of

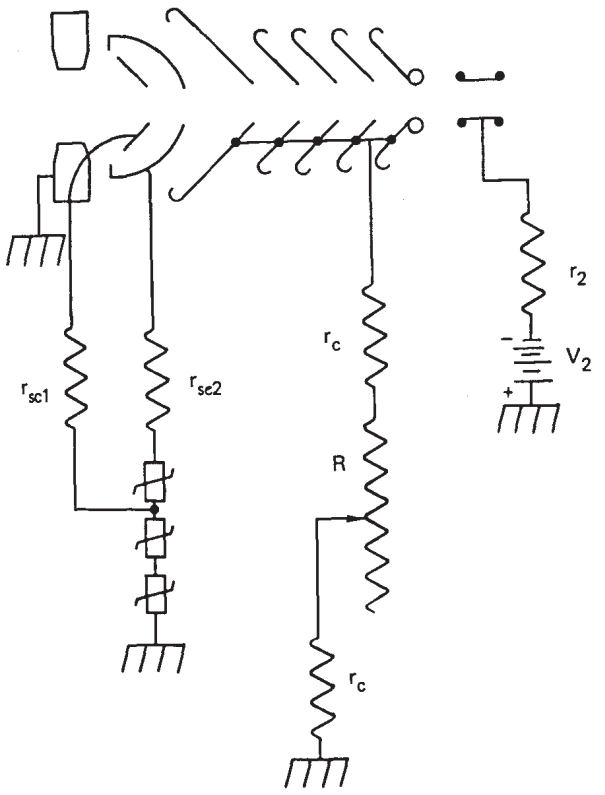


Fig. 11. The electrical circuit used with magnetic electron suppression. The number of nonlinear resistors was varied to select electron catcher voltages up to +18 kV.

nonlinear resistors as voltage limiters, since the catcher tended to go to a high positive potential. This tendency for positive potential was apparently due to the scraping off of the outer part of the ion beam as the beam diverged. With a hydrogen beam, this might have been due partly to the faster divergence of the fractional energy ions. Since scrape off of beam was also observed with a $He^+$ beam, the main effect must be the divergence.

The collector current $I_c$ and voltage $V_c$ varied during a pulse in a reproducible manner. During the first 50 to 100 ms, while the pressure rise was fastest, $V_c$ dropped by about 20 kV to about 50 kV and then decayed at a much slower rate for the remainder of the pulse. Also, the ac ripple in the accel current to the source appeared on $I_c$ and $V_c$ and was amplified by a factor that varied during the pulse. The amplification factor passed through a maximum value of about three as the collector voltage passed through a value of about 50 kV. When the load resistor $R$ was set high so that $V_c$ stayed above 50 kV, the ac ripple increased during the pulse as $V_c$ decayed toward 50 kV. When $R$ was set low, the ripple decreased during the pulse as $V_c$ decayed below 50 kV. The nonlinear resistors that were used to control the voltages of the two electron catchers were effective in suppressing any voltage ripple at those electrodes.

The greatest distinction between the results with electrostatic suppression (ES) and those with magnetic suppression (MS) was that the maximum net current $I_c$ to the collector was lower with MS. This could be due to the collection of either fewer ions or more electrons.

The efficiency of the BDC with MS was 40% at the beginning of a pulse of the hydrogen beam but dropped to 23% at the end of a 300-ms pulse. A plot of $I_c$ versus $V_c$ is shown in Fig. 12; comparison with Fig. 10 shows a lower efficiency with MS than with ES. In both cases, the stated efficiency was based on the total ion power, including the fractional energy ions. It can be seen in Fig. 12 that the collected current, $I_c$, increased rapidly with collector voltage, $V_c$, near $V_c = 0$. That indicates that an electric field is indeed needed in combination with the magnetic field to remove the electrons and allow the MS concept to work.

Figure 12 also show the $I_c$ versus $V_c$ curve measured with a $He^+$ beam. Again, comparison with Fig. 10 shows that less net current was collected with MS than with ES. The efficiency with a $He^+$ beam and MS was 37% early in the pulse but dropped to 19% at the end of a 500-ms pulse, nearly the same as with a hydrogen beam. We speculate that the losses due to

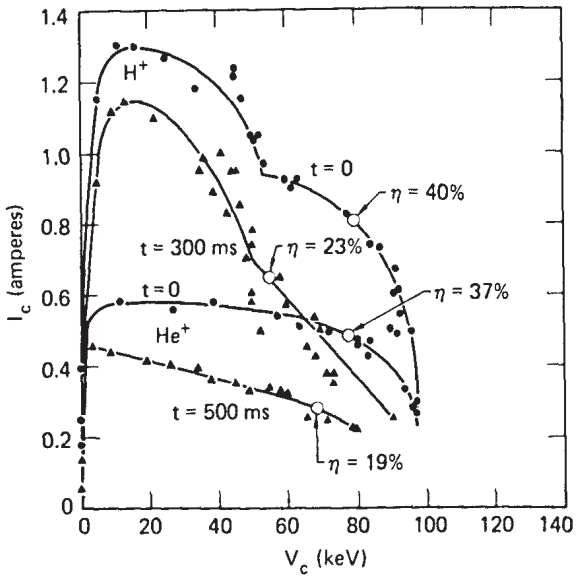


Fig. 12. Measured collector current $I_c$ vs collector voltage $V_c$ for a hydrogen beam and for a helium beam, both using magnetic suppression. Improvements in the electron catcher should increase the recovery efficiency to more nearly equal that with electrostatic suppression (Fig. 10).

the greater secondary electron emission with $He^+$ were nearly balanced by the losses due to the fractional energy ions with hydrogen. The secondary emission coefficient is about three times greater for $He^+$ on Mo than for either $H^+$ or $H_2^+$ on Mo.

## 7. SCALING TO A FUSION REACTOR

The 0.7 MW/m of residual ion beam used in the test is scalable to the 2-to-4 MW/m (steady state) needed for fusion reactors, but is still well below the 12 MW/m (pulsed) in the injectors for TFTR. In Fig. 13, the dashed curve shows the calculated[1] efficiency, $\eta$, for 100 keV $D^+$ plotted here as a function of ion power per linear meter, $P/l$. The efficiency decreases as the ion power increases because of the greater suppressor voltage and the greater loss currents with more intense beams. The dashed curve was calculated for the configuration where the source and the ion collector are held at high positive potential, and was normalized to one of our sets of data. The average of our measured efficiency, $\eta = 65 \pm 7\%$, is indicated. With the source, and therefore the ion collector, operated at near-ground potential, the transmitted ions would be recovered, and therefore the efficiency would be about 15% higher, as shown by the solid curve. The location of the direct converters for the injectors for the three devices, TFTR, MFTF, and JXFR, are indicated, although the fact that their energies are different from the assumed 100 keV causes them to be displaced from the curve. Figure 14 shows an artist's drawing of a neutral-beam

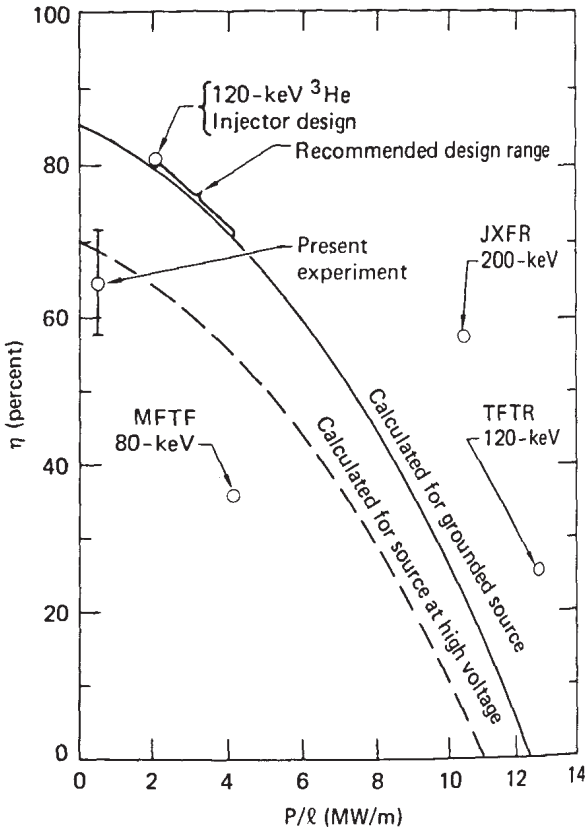


**Fig. 13.** The efficiency ($\eta$) of direct recovery plotted against the beam ion power per linear meter ($P/l$). For the dashed curve, the transmitted ions are assumed to be lost as was true in the experiment (indicated with its error bar). With a source operated near ground potential the transmitted ions are recovered, increasing the efficiency by 15%. The location of three large devices is indicated, although their different energies prevent them from falling on the 100 keV $D^+$ curves plotted. Also indicated is the location of a 120 keV $^3He$ neutral-beam injector designed for heating fusion reactor plasmas.[4] Steady state injectors should be designed for the range from 2 to 4 MW/m.

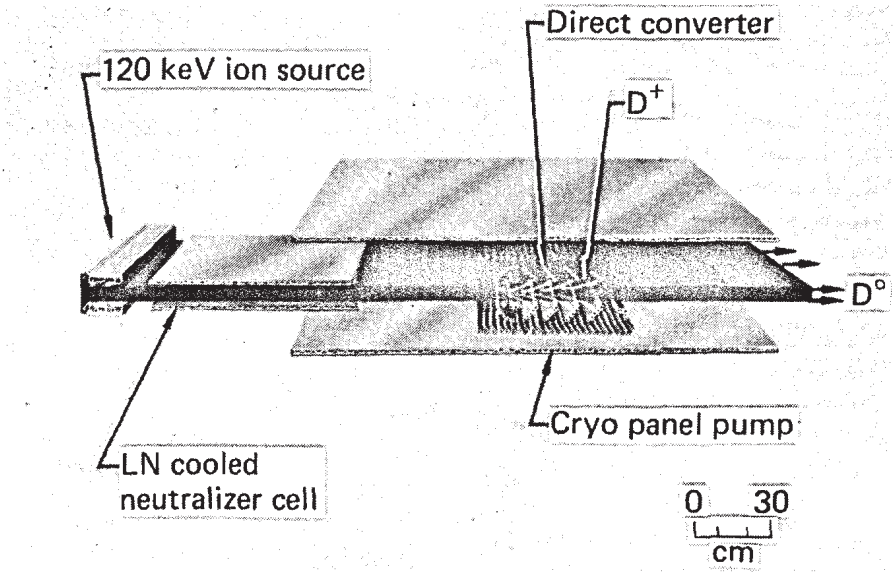


**Fig. 14.** An artist's drawing of a neutral-beam injector for steady-state reactor application. The cryopanels and the cooling of the neutralizer reduce the gas density at the direct converter.

injector for steady-state reactor application. The cryopanels and cooled neutralizer reduce the gas pressure at the direct converter to the required range ($p < 2 \times 10^{-5}$ Torr), as discussed above.

## 8. CONCLUDING REMARKS

The work reported here gave a reasonably high efficiency of power recovery, measured at high-voltage and high-ion beam power. The 0.7 MW/m of residual ion beam used in the test is scalable to the 2-to-4 MW/m (steady state) needed for fusion reactors, but is still well below the 12 MW/m (pulsed) in the full scale injectors developed for TFTR. The average measured efficiency was $\eta = 65 \pm 7\%$ at the beginning of a pulse while the vacuum was good. If the source, and therefore the ion collector, had been operated at near-ground potential, the transmitted ions would have been recovered and the efficiency increased by about 15%.

We now believe that the reason that the results were not better in our previous direct converter tests with a pulsed, high-power beam was the incomplete conditioning of metal surfaces. In the test reported here, all of the electrodes were designed to run hot and therefore remain free of gas. Also, the testing period was much longer than any of our previous tests. One reason why cleanup requires so much time in a test is that many parameters are varied. The variation of almost any of the parameters produces outgassing from a new area. In an operating direct converter with all controllable parameters fixed, the cleanup should be faster.

The measured efficiency with magnetic suppression was not as high as with electrostatic suppression. Further testing is needed, but we expect that magnetic suppression can be made to yield higher efficiency than electrostatic suppression on higher power beams.

## ACKNOWLEDGMENTS

The authors wish to thank A. F. Lietzke for supervising the operation of the beam and for his help with the experiment. We also want to thank the other members of the Berkeley beam group, especially H. M. Owren and K. H. Berkner, for their interest and support. Finally, we gratefully acknowledge J. D. Kinney and M. C. Fowler for their technical support and W. R. Call and T. H. Batzer for building and operating the cryopump. We appreciate the many iterations of numerical calculations by T. C. Chu. This work was performed under the auspices of the U. S. Department of Energy by the Lawrence Livermore National Laboratory under Contract W-7405-Eng-48.

## REFERENCES

1. W. L. Barr, R. W. Moir, and G. W. Hamilton, Test results on a high-power, 100-keV beam direct converter, Lawrence Livermore National Laboratory Report UCRL-84432 (1980).
2. W. L. Barr, R. W. Moir, G. W. Hamilton, and A. F. Lietzke, Tests of high-power direct conversion on beams and on plasma, in *Proc. Eighth Symp. Engineering Problems of Fusion Res.*, San Francisco, Calif. (IEEE, 1979).
3. W. L. Barr and R. W. Moir, Test results on plasma direct converters, *Nucl. Technol./Fusion*, to be published.
4. A. S. Blum, W. L. Barr, W. L. Dexter, J. H. Fink, R. W. Moir, and T. P. Wilcox, Design study of a 120-keV, $^3$He neutral-beam injector, *J. Fusion Energy* **1**:69 (1981).
5. W. L. Barr, J. N. Doggett, G. W. Hamilton, J. D. Kinney, and R. W. Moir, Engineering of beam direct conversion for a 120-kV, 1-MW ion beam, in *Proc. Seventh Symp. Engineering Problems of Fusion Res.*, Knoxville, Tenn. (IEEE, 1977).
6. P. A. Raimbault, Analytical and numerical analysis of energy recovery systems for neutral-beam injectors, EUR-CEA-FC-899, Report (1977).
7. W. K. Dagenhart et al., Direct energy conversion of un-neutralized ion beams with close-coupled electric and magnetic fields, in *Proc. IEEE Int. Conf. Plasma Sci.*, Madison, Wisc. (IEEE, 1980).
8. W. S. Cooper, High-energy neutral injector with direct energy recovery, Lawrence Berkeley Laboratory Report UCID-7310 (1975).
9. E. Thompson, J. R. Coupland, D. Dirmikis, D. P. Hammond, and A. J. T. Holmes, The development of neutral injection to the megawatt power level, in *Proc. Sixth Symp. Engineering Problems of Fusion Res.*, San Diego, Calif. (IEEE, 1975).
10. K. Hashimoto, K. Sinya, O. Morimiya, J. Ohmori, H. Ohguma, E. Ishii, and H. Yamato, The design study of neutral-beam injection system for JXFR, in *Proc. Eighth Symp. Engineering Problems of Fusion Res.*, San Francisco, Calif. (IEEE, 1979).
11. H. Verbeek, in *Radiation Effects on Solid Surfaces* edited by M. Kaminsky, ed. (American Physical Society, Washington, D.C., 1976), chap. 10. O. C. Oen and M. T. Robinson, *Nucl. Instrum. Methods* **132**:647–653 (1976).
12. S. Hamasaki, R. C. Davidson, N. A. Krall, and P. C. Liewer, *Nucl. Fusion* **15**:27–33 (1975).
13. T. H. Batzer, R. E. Patrick, and W. R. Call, A neutral-beam-line pump with helium cryotrapping capability, Lawrence Livermore National Laboratory Report UCRL-81196 (1978).